AUTHOR(S): SINGH, N.K., YADAV, M.K. and FERNANDEZ, C.

TITLE: Electrocatalytic properties of La1-xCuxCoO3 (0 <= X <= 0.8) film electrodes prepared by Malic Acid sol -gel method at pH=3.75.

YEAR: 2017

Publisher citation: SINGH, N.K., YADAV, M.K. and FERNANDEZ, C. 2017. Electrocatalytic properties of La1-xCuxCoO3 (0 <= X <= 0.8) film electrodes prepared by Malic Acid sol -gel method at pH=3.75. International journal of electrochemical science [online], 12(8), pages 7128-7141. Available from: https://doi.org/10.20964/2017.08.68

OpenAIR citation: SINGH, N.K., YADAV, M.K. and FERNANDEZ, C. 2017. Electrocatalytic properties of La1-xCuxCoO3 (0 <= X <= 0.8) film electrodes prepared by Malic Acid sol -gel method at pH=3.75. International journal of electrochemical science, 12(8), pages 7128-7141. Held on OpenAIR [online]. Available from: https://openair.rgu.ac.uk

Int. J. Electrochem. Sci., 12 **(2017)** 7128 – 7141, doi: 10.20964/2017.08.68

International Journal of ELECTROCHEMICAL SCIENCE
www.electrochemsci.org

Electrocatalytic Properties of $La_{1-x}Cu_xCoO_3$ ($0 \leq X \leq 0.8$) Film Electrodes Prepared by Malic Acid Sol -Gel Method at pH = 3.75

N. K. Singh[1,*], *M. K. Yadav*[1] *and Carlos Fernandez*[2]

[1] Deapartment of Chemistry, Faculty of Science, University of Lucknow, Lucknow-226007, INDIA
[2] School of Pharmacy and Life Sciences, Robert Gordon University, Aberdeen, UK-AB10 7GJ
[*]E-mail: nksbhu@yahoo.com, singh_narendra@lkouniv.ac.in

Received: 29 April 2017 / *Accepted:* 12 June 2017 / *Published:* 12 July 2017

La-based Perovskite-type oxides with composition $La_{1-x}Cu_xCoO_3$ ($0 \leq X \leq 0.8$) have been synthesized by malic acid sol-gel low temperature route at pH 3.75. In each preparation, nitrate salts of lanthanum, copper, cobalt and malic acid were taken as starting material. The pH of the solution was adjusted by using ammonia solution. Techniques used to know the physical properties of the materials were scanning electron microscope (SEM) powder X-ray diffraction (XRD). All the electrochemical *viza* cyclic voltammetry, roughness factor and anodic polarization studies have been performed in three electrode single compartment glass cell. For the purpose, materials were transferred in the form of oxide film electrode on Ni conducting support. XRD data showed the formation of almost pure phase of the material with hexagonal crystal geometry. The cyclic voltammetric study showed that each oxide electrode exhibited a pair of redox peaks prior to the oxygen evolution reaction (OER). The values of Tafel slope (78-90 mV $decade^{-1}$) and reaction order (~ 1) indicate that each catalyst follows similar mechanistic path. The data of anodic polarization study shows that the substitution of Cu in place of La in the base oxide increases the electrocatalytic activity considerably. The value was found to be highest with 0.4 mol Cu substitution. Electrochemically active area of the material was determined in terms of roughness factor by recording the cyclic voltammograms at different scan rates in the potential region 0.0-0.1V. The roughness factor was observed to be highest with 0.2 mol Cu-substituted oxide.

Keywords: Perovskite-type oxide, malic acid sol-gel, XRD, Electrocatalytic activity, Thermodynamic parameters, roughness factor

1. INTRODUCTION

The day-to-day increase in the global energy demand and environmental pollution created by

fossil fuels (coal, petroleum, etc.) has a great task to researchers for the development of clean and sustainable energy conversion and storage systems [1,2]. Due to sluggish kinetics of both oxygen reduction reaction (ORR) and oxygen evolution reaction (OER), the investigations of efficient electrocatalysts has been a topic of importance during last few decades for the development of new generation of energy technologies like fuel cells, metal air batteries, hydrogen production from water and solar fuel synthesis [3-7]. Consequently, great efforts have been devoted and produced electrocatalysts which are mainly based on pure metal, metal oxides, mixed metal oxides having spinel and perovskite structure and studied intensively [8]. The perovskite-type oxides of lanthanum are found to be very promising materials towards active electrocatalysts in many technological reactions like electrolytic evolution (reduction) of oxygen [9-13], the oxidation of CO and hydrocarbon and the reduction of nitrogen oxides [14]. It is also well known that the electrocatalytic properties of the material are strongly influenced by the preparation methods, temperature, metal ion substitution and pH of the precursor solution. The literature showed that high temperature methods, like ceramic and thermal decomposition [15-20] produced oxides with low specific surface area and hence very low electrocatalytic properties.

In order to improve the physicochemical and electrocatalytic properties of the materials, some low temperature synthetic routes [21-25] based on amorphous organic acids (malic, citric, steric, polyacrylic acid), hydroxide and cyanide solid solutions etc. have been adopted by the researchers. By using these low temperature synthetic routes, Singh et al. [9, 26-36] reported an improved electrocatalytic properties of pure and substituted Co, Mn and Ni-based lanthanum perovskite with regards to oxygen evolution reaction in alkaline medium. Very recently [37-41], some La-based perovskite-type oxides have been reported as electrocatalysts for oxygen evolution as well as oxygen reduction. Singh et al [32] studied the electrocatalytic properties Sr-substituted $LaMnO_3$ obtained by low temperature malic acid sol-gel route [21] at pH = 3.5 and found very good electrocatalytic activity for oxygen evolution in alkaline medium. In view of above, we produced Cu-substituted lanthanum cobaltates by using the similar synthetic procedure [21, 32] at pH = 3.75 and studied their physicochemical and electrocatalytic properties with regards to oxygen evolution reaction in alkaline medium. Results, so obtained, are described in this paper.

2. EXPERIMENTAL

Perovskite-type oxides of La, Cu and Co having composition $LaCoO_3$, $La_{0.8}Cu_{0.2}CoO_3$, $La_{0.6}Cu_{0.4}CoO_3$, $La_{0.4}Cu_{0.6}CoO_3$, and $La_{0.2}Cu_{0.8}CoO_3$ were prepared by low temperature malic acid sol-gel route [21]. Chemical and reagents used in each preparation were purified and analytical grade and purchased from Merck and Qualigens. The required amounts of metals nitrate as per stoichiometric ratio of the composition of oxide material were weighed and dissolved in 500 ml double distilled water. An excess amount of malic acid was added to this solution. The pH of the solution was maintained to 3.75 by using 28% ammonia solution. The solution was then concentrated on water bath at temperature about 80°C. A gel like mass obtained was decomposed at higher temperature. Further,

the material was crushed into agate pastel mortar to get the fine powder, which was finally sintered at 650 °C for 5 hr in a PID controlled electrical furnace (ASCO, India) to obtain the desired oxide.

X-ray diffraction pattern (XRD) was recorded to confirm the perovskite phase of the material using XPERT-PRO Diffractometer (Model PW3050/60; Radiation Source: Cu-Kα; λ = 1.54048 Å). The morphology of the oxide film on Ni was examined by scanning electron microscope (JOEL JSM 6490LV). For electrochemical characterization, oxide powder was transformed in the form of film electrode on Ni-support by adopting oxide slurry painting technique. For the purpose, slurry of the oxide powder was prepared with few drops of non-ionic detergent Triton X-100. This slurry was then painted to one side of the pre-treated Ni plate (area = 1.5 cm^2) and subsequently heat treated at 380 °C for 1½ hr. The process was repeated 2-3 times to obtain the desired loading on the conducting support. The electrical contact with the oxide film was made by using copper wire, silver paste and Araldite epoxy. The treatment of Ni-support and electrical connection with the oxide film to form the oxide film electrode were done in the same way as described earlier [26, 31]. All the electrochemical studies such as cyclic voltammetry, double layer capacitance and anodic polarization curve were performed in a three electrode single compartment glass cell using an electrochemical work station (Gamry Reference 600 ZRA) provided with potentiostat/galvanostat. Two software, corrosion and physical electrochemistry were used for electrochemical studies and data were recorded on the desktop computer (HP). A platinum foil (~2 cm^2) and Hg/HgO/1M KOH (E° = 0.098 V vs NHE at 25°C) were taken as auxiliary and reference electrode, respectively. The working electrode was the oxide film electrode. A Luggin capillary (agar-agar and potassium chloride gel) was employed to make the connection between working and reference electrode. This arrangement was done to minimize the solution resistance (iR drop) between the working and reference electrode. The formal overpotential values mentioned in the data were obtained by the relation, $\eta = E - E_{O_2/OH^-}$, where E and E_{O_2/OH^-} (= 0.303 V vs. Hg/HgO) [42] are the applied potential across the catalyst/ 1 M KOH interface and the theoretical equilibrium Nernst potential in 1 M KOH at 25 °C, respectively.

3. RESULT AND DISCUSSION

3.1 Physicochemical Properties

3.1.1 Scanning Electron Micrograph (SEM)

SE-micrographs of pure and Cu substituted $LaCoO_3$ sintered (at 650°C) oxide film on Ni support is shown in Fig. 1(a-e) at magnification ×500. From figure it is observed that morphology of each oxide film was found to be almost similar regardless of the Cu-substitution in the base oxide.

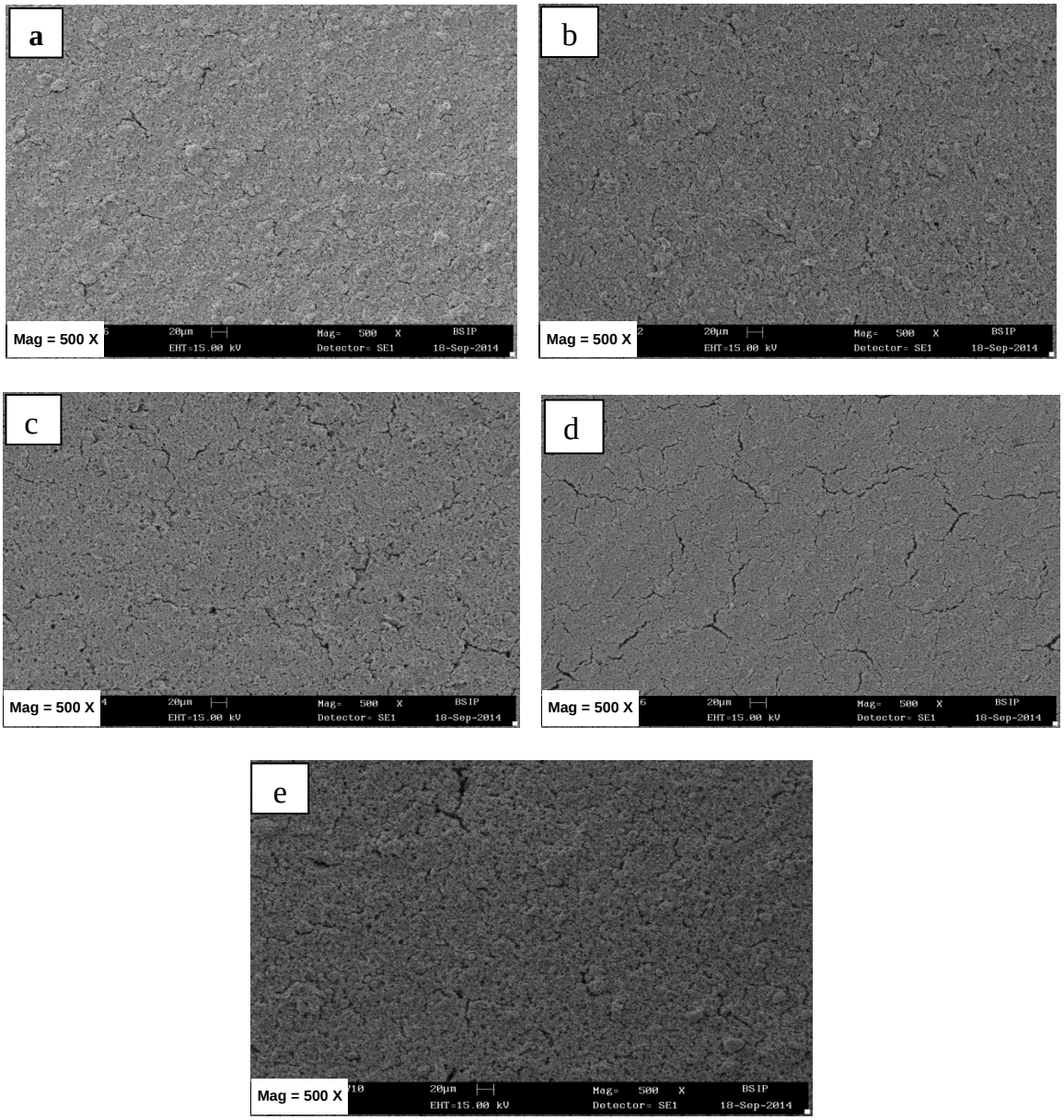

Figure 1. SE Micrographs of oxide film on Ni-support; a: $LaCoO_3$, b: $La_{0.8}Cu_{0.2}CoO_3$, c: $La_{0.6}Cu_{0.4}CoO_3$, d: $La_{0.4}Cu_{0.6}CoO_3$, e: $La_{0.2}Cu_{0.8}CoO_3$

The appearance of the oxide film is found to be compact and homogeneous throughout. Some small cracks are also observed in the oxide film.

3.1.2 X-ray diffraction (XRD)

The powder XRD pattern of $LaCoO_3$ and its 0.4 mol Cu-substituted oxide material (sintered at 650°C for 5 hr) was taken in 2θ range 20° to 80° using a Philips X-ray Diffractometer having Cu-Kα (λ= 1.54184 Å) as a radiation source. The spectra, so obtained, are represented in Fig. 2. The 2θ and the corresponding 'd' values of the diffraction lines as shown in Fig. 2 were found to be best match with JCPDS ASTM file 25-1060 for $LaCoO_3$ and followed hexagonal crystal geometry.

The crystallite size of the material was calculated by using the Scherer's formula [43] and found to be 32, 24 nm, respectively with x = 0 and 0.4 mol Cu-substituted oxides.

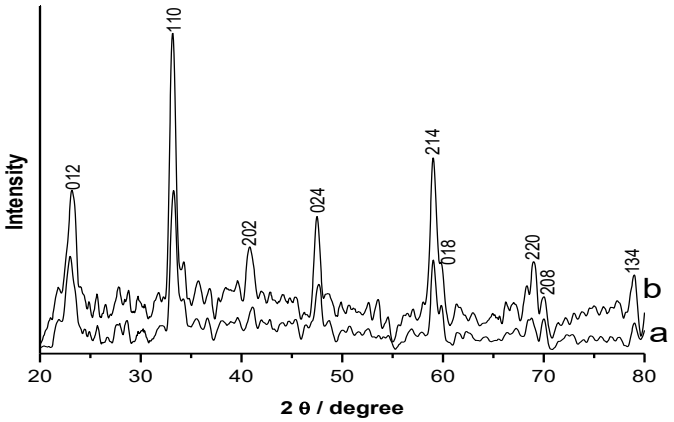

Figure 2. X-ray diffraction patterns of $La_{1-x}Cu_xCoO_3$, sintered at 650°C for 5 h; (a) x = 0 mol (b) x = 0.4 mol

3.2. Electrochemical properties

3.2.1. Cyclic Voltammetry (CV)

Cyclic voltammograms of the synthesized oxide film electrodes, recorded between the potential window 0.0-0.7V at the scan rate of 20 $mVsec^{-1}$ at 25 °C in 1 M KOH solution, are shown in Fig. 3. Nature and characteristics of the voltammograms of each oxide electrode material appeared to be similar.

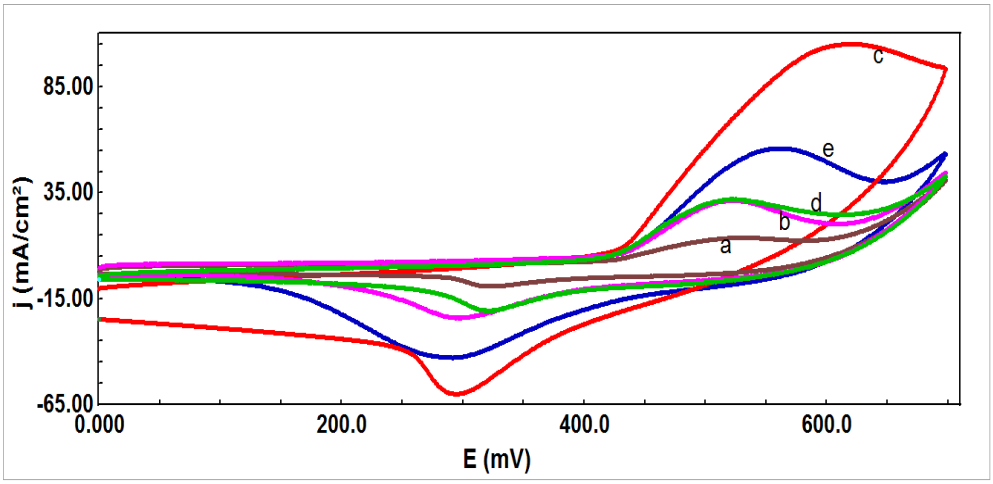

Figure 3. Cyclic voltammograms of pure and Cu-substituted film electrode on Ni at scan rate of 20 mV/sec in 1M KOH (25°C); a: $LaCoO_3$, b: $La_{0.8}Cu_{0.2}CoO_3$, c: $La_{0.6}Cu_{0.4}CoO_3$, d: $La_{0.4}Cu_{0.6}CoO_3$, e: $La_{0.2}Cu_{0.8}CoO_3$.

Each curve shows two redox peaks, an anodic and corresponding cathodic one. Values of peak potentials (E_{Pa} & E_{Pc}), peak separation potential ($\Delta E_P = E_{Pa} - E_{Pc}$) and formal redox potential {$E° = (E_{Pa} - E_{Pc})/2$} are listed in Table 1.

The anodic peaks (E_{Pa} = 566±44 mV) and their corresponding cathodic peaks (E_{Pc} = 306±16 mV), prior to the onset of oxygen evolution reaction, were found to be very similar to that observed in literature [26, 31, 44]. Values of the anodic and cathodic peak potential ($E_{Pa} \approx 490$ mV and $E_{Pc} \approx 380$ mV) in 1 M KOH for bare Ni [45] indicate that the redox peaks observed for the oxide electrodes result from the Ni substrate which might come in contact with the electrolyte during cycling process. Also, oxides prepared at low temperature undergo hydration [46] easily in solution and electrolyte may come in contact with the substrate through pores, cracks and grain boundaries.

Table 1. Values of the Cyclic Voltammetric parameters of Ni/ $La_{1-x}Cu_xCoO_3$ ($0 \leq X \leq 0.8$) in 1 M KOH at 25 °C (scan rate = 20 mV sec^{-1}).

Electrode	**E_{Pa} / mV**	**E_{Pc} / mV**	**ΔE_p / mV**	**$E° = (E_{Pa}+E_{Pc})$ / 2 / mV**
$LaCoO_3$	532	322	210	427
$La_{0.8}Cu_{0.2}CoO_3$	523	296	227	409
$La_{0.6}Cu_{0.4}CoO_3$	610	294	316	452
$La_{0.4}Cu_{0.6}CoO_3$	523	321	202	422
$La_{0.2}Cu_{0.8}CoO_3$	553	289	264	421

The cyclic voltammetric curves were also recorded at varying scan rates of 20, 40, 60, 80, 100 and 120 mV sec^{-1} in 1M KOH at 25°C in the potential region 0.0-0.7V. A representative cyclic voltammogram for 0.8 mol Cu-substituted electrocatalysts is shown in the Fig. 4.

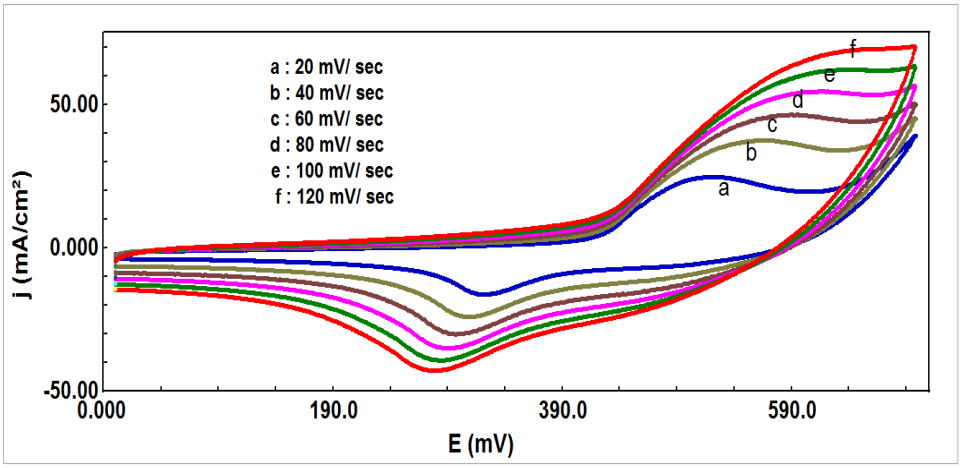

Figure 4. Cyclic voltammograms of the Ni/$La_{0.2}Cu_{0.8}CoO_3$ film electrode at different scan rates in 1M KOH (25°C).

The estimated voltammetric parameters are shown in the Table 2 for base and 0.8 mol Cu-substituted oxide. The nature of CV curve observed at different scan rates was found to be similar to that observed at scan rate of 20 mV sec $^{-1}$. But, both anodic and cathodic peaks shifted either side with the variation of scan rate between 20 to 120 mV sec^{-1}. This indicates the quasireversible nature of the redox process. The observed shift in the anodic and the cathodic peak potentials were found to be 132-156 mV and 33-94 mV towards positive and negative directions, respectively. The scan rate also influenced the anodic and cathodic peak currents. It increases both anodic and cathodic peak current values linearly with increase in the scan rates and ratio anodic and cathodic peak current was found to be more than unity. This indicates that redox process is irreversible.

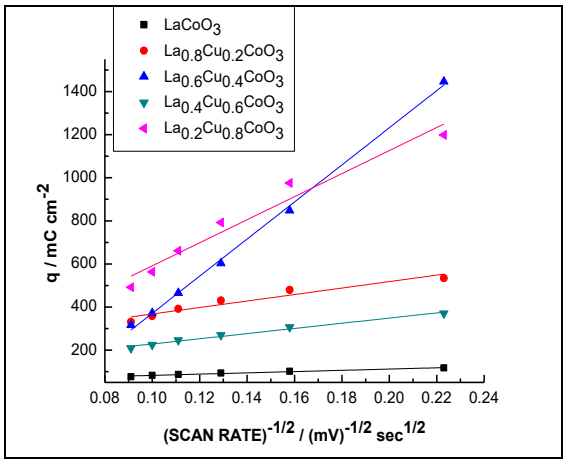

Figure 5. Plot of voltammetric charge (q) vs (scan rate)$^{-1/2}$ for $La_{1-x}Cu_xCoO_3$ ($0 \leq x \leq 0.8$) films on Ni in 1M KOH (25°C).

Table 2. Cyclic Voltammetric parameters for the $La_{1-x}Cu_xCoO_3$ (x = 0 and 0.8) film electrode on Ni in 1 M KOH at 25°C.

Scan rate /mVsec^{-1}	**E_{Pa} /mV**	**E_{Pc} /mV**	**$\Delta E = E_{Pa} - E_{Pc}$ /mV**	**$E° = (E_{Pa} + E_{Pc})/2$ / mV**	**$\|j_{Pa}\|$ /mA cm^{-2}**	**$\|j_{Pc}\|$ /mA cm^{-2}**	**$\|j_{Pa}\| / \|j_{Pc}\|$**	**q /mC cm^{-2}**
20	553 (532)	289 (322)	264 (210)	421 (427)	70.2 (13.7)	60.1 (9.2)	1.3 (1.5)	1198.9 (117.0)
40	600 (561)	259 (310)	341 (251)	429 (435)	103.1 (21.5)	81.2 (13.8)	1.3 (1.5)	975.8 (101.4)
60	641 (588)	238 (303)	403 (285)	440 (445)	127.3 (28.9)	97.9 (17.6)	1.3 (1.6)	792.0 (93.2)
80	665 (618)	221 (295)	444 (323)	443 (456)	147.4 (35.0)	110.7 (20.7)	1.3 (1.7)	661.0 (87.2)
100	681 (645)	205 (296)	476 (349)	443 (471)	164.1 (41.9)	120.5 (23.4)	1.4 (1.8)	562.7 (82.7)
120	687 (666)	195 (289)	492 (377)	441 (477)	176.0 (48.8)	128.5 (26.0)	1.4 (1.9)	491.3 (76.3)

(Values given in parenthesis correspond to $LaCoO_3$)

3.2.2. Roughness Factor (R_F)

Electrochemically active area of oxide materials was determined by recording the CV curves in the potential window 0.0 to 0.1 V at varying scan rates of 20, 40, 60, 80, 100 and 120 mV Sec^{-1}. A representative curve is shown in Fig. 6 for $La_{0.2}Cu_{0.8}CoO_3$ electrode. Values of capacitive current (j_{cap}) were estimated at the middle (50 mV) of the CV curve at each scan. A plot was constructed between current and scan arte (Fig. 7).

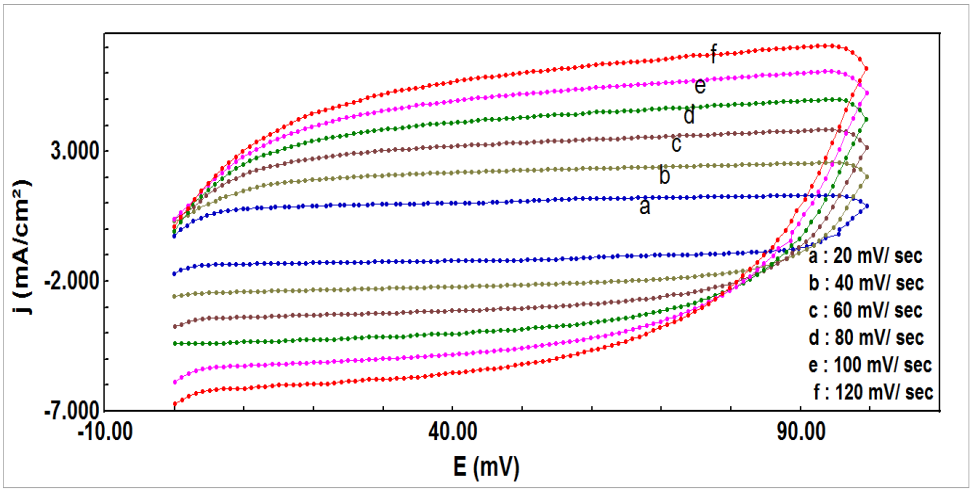

Figure 6. Cyclic voltammograms for $Ni/La_{0.2}Cu_{0.8}CoO_3$ electrode in the potential region 0.0-0.1 V in 1 M KOH (25°C),

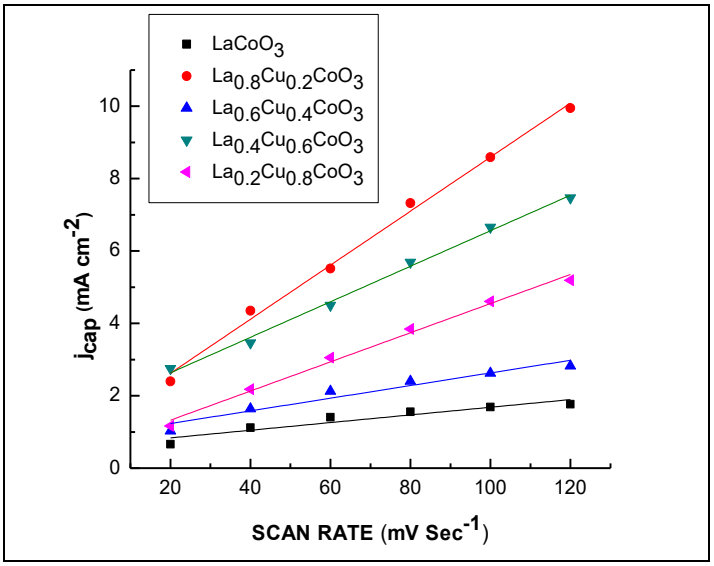

Figure 7. Plot of capacitive current density (j_{cap}) *vs.* scan rate for $La_{1-x}Cu_xCoO_3$ ($0 \leq x \leq 0.8$) in 1 M KOH (at 25°C)

The slope of the straight line gives the value of capacitance double layer (C_{dl}). The corresponding roughness factor was calculated by assuming the double layer capacitance of the smooth oxide surface 60 µF cm^{-2} [47] and the values, so obtained, is given in Table 3. From table 3, it is

observed that oxide roughness factor has no any trend with Cu-substitution in the base oxide. It was found to be maximum with 0.2 mol Cu-substitution and minimum with base oxide.

3.2.3 Electrocatalytic activity

The iR compensated anodic polarization curves (E vs.log j) recorded at a scan rate of 0.2 mV sec^{-1} for pure and copper doped perovskite film electrode on Ni in 1M KOH at 25 °C is represented in Fig. 8. To compare the electrocatalytic activities of electrodes, the observed values of Tafel slope (b) and current density at two overpotentials (347 & 447 mV) as well as overpotential at three different current density (10, 100 and 300 $mAcm^{-2}$) are given in Table 3. Nature of the polarization curve for each oxide electrode was similar with almost same Tafel slope ranged between 78-90 mV $decade^{-1}$.

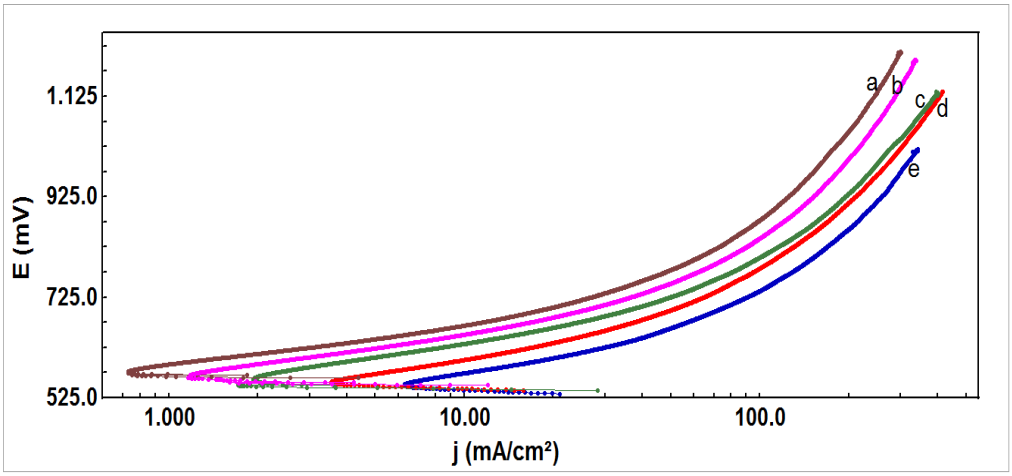

Figure 8. Tafel plots for the pure and Cu-substituted $LaCoO_3$ film electrode on Ni in 1M KOH (25°C); scan rate: 0.2mVsec^{-1}; a: $LaCoO_3$, b: $La_{0.8}Cu_{0.2}CoO_3$, c: $La_{0.4}Cu_{0.6}CoO_3$, d: $La_{0.2}Cu_{0.8}CoO_3$, e: $La_{0.6}Cu_{0.4}CoO_3$

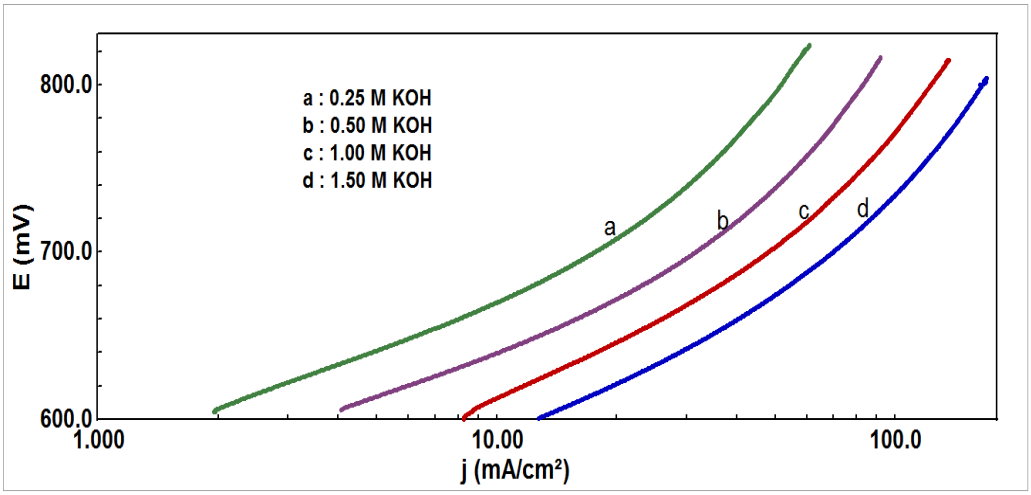

Figure 9. Tafel plot for the $La_{0.6}Cu_{0.4}CoO_3$ film electrode on Ni in varying KOH concentrations (μ = 1.5) at 25°C.

To determine the order of electrochemical reaction, the polarization curves were recorded in varying KOH concentrations (0.25-1.5M) at 25 °C. The ionic strength (μ = 1.5) of the solution was kept by using inert electrolyte KNO_3. A representative curve for $La_{0.6}Cu_{0.4}CoO_3$ is shown in the Fig. 9. The nature of anodic polarization curves at varying KOH concentration was similar for each oxide electrode studied. The plot log j vs. log [OH^-], as shown in the Fig. 10 for $La_{0.6}Cu_{0.4}CoO_3$ was constructed at different applied potentials. The order of reaction was calculated by measuring the slope of the plot. Values of the order of reaction were found to be almost unity in each case and are given the Table 3.

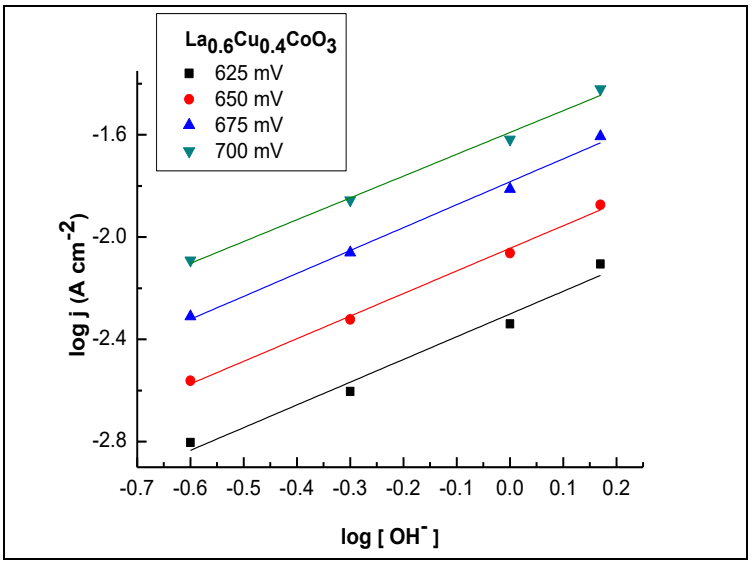

Figure 10. Plot of log j vs log [OH^-] at a different applied potential for $La_{0.6}Cu_{0.4}CoO_3$ film electrode on Ni at 25°C.

Table 3. Electrode kinetic parameters for oxygen evolution reaction on $La_{1-x}Cu_xCoO_3$ ($0 \leq x \leq 0.8$) electrodes in 1 M KOH at 25°C

Electrode	Tafel slope / mVd^{-1}	Roughness Factor (R_F)	Order (p)	η_{O_2} / mV at j_a (mA cm^{-2})			j_a (mA cm^{-2}) at η_{O_2} / mV	
				10	100	300	347	447
$LaCoO_3$	78	176	~1	364	571	901	7.0	39.9
$La_{0.8}Cu_{0.2}CoO_3$	80	1244	~1	345	541	839	10.3	49.2
$La_{0.6}Cu_{0.4}CoO_3$	90	291	~1	268	431	648	44.5	111.6
$La_{0.4}Cu_{0.6}CoO_3$	88	818	~1	333	519	780	14.3	59.3
$La_{0.2}Cu_{0.8}CoO_3$	90	671	~1	297	479	715	27.7	70.2

Among the oxide film electrodes prepared by this method at pH = 3.75, it has been found that the $La_{0.6}Cu_{0.4}CoO_3$ is the electrocatalytically most active, while the base is the least active. This indicates that the Cu-substitution increased the oxide electrocatalytic activity considerably. Based on the apparent current density data at constant overpotential (η_{O_2} = 447mV), the different electrocatalysts show the order as:

$La_{0.6}Cu_{0.4}CoO_3$ (j_a= 111.2 mAcm^{-2}) > $La_{0.2}Cu_{0.8}CoO_3$ (j_a= 70.2 mAcm^{-2}) > $La_{0.4}Cu_{0.6}CoO_3$ (j_a= 59.2 mAcm^{-2}) > $La_{0.8}Cu_{0.2}CoO_3$ (j_a= 49.2 mAcm^{-2}) > $LaCoO_3$ (j_a= 39.9 mAcm^{-2})

The thermodynamic parameters for the oxygen evolution reaction on pure and copper doped $LaCoO_3$ perovskite oxide film electrode was determined by recording the polarization curves for in 1M KOH at varying temperatures (20°-50°C). The temperature of the reference electrode was kept constant (25°C) during the experiment. A representative polarization curve is shown in the Fig. 11 for 0.4 mol copper doped $LaCoO_3$. From the polarization curve data, the Arrhenius plot, log j vs 1/T (Fig. 12) was constructed at different constant potentials. The slope of straight lines gives the activation energy.

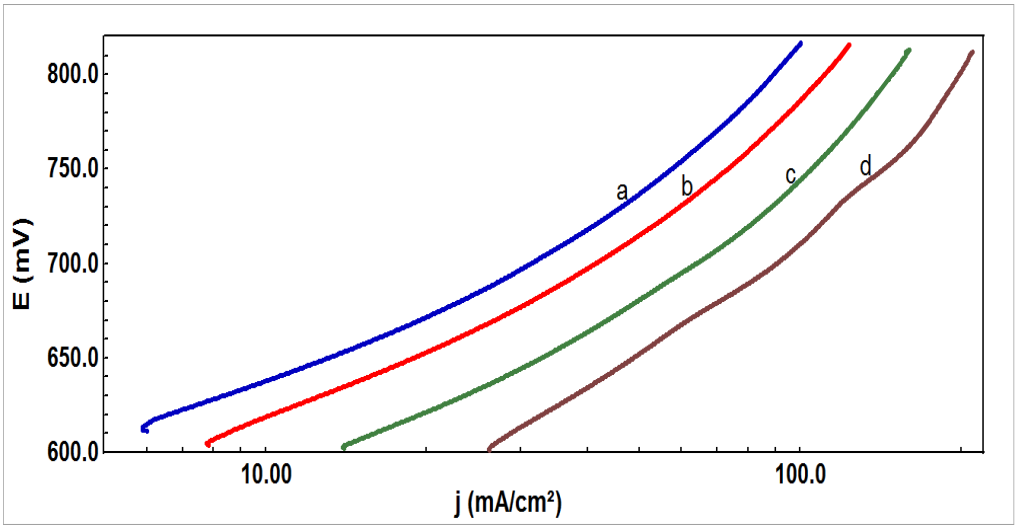

Figure 11. Tafel plot for the $La_{0.6}Cu_{0.4}CoO_3$ film electrode on Ni at different temperatures in 1 M KOH; a: 20 °C, b: 30 °C, c: 40 °C, d: 50 °C.

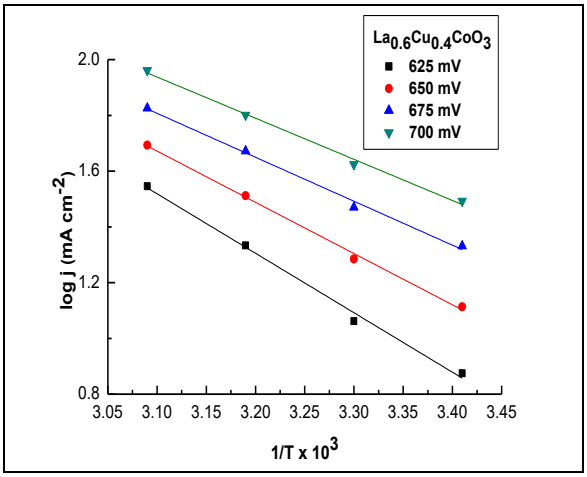

Figure 12. The Arrhenius plot for $La_{0.6}Cu_{0.4}CoO_3$ film electrode on Ni in 1 M KOH at different applied potential.

Other thermodynamic parameters such as $\Delta H^{\circ\#}$ and $\Delta S^{\circ\#}$ [48] were calculated by using following relations;

$\Delta H_{el}^{\circ\#} = \Delta H^{\circ\#} - \alpha F\eta$ …….. (1)

Where, α (transfer coefficient) = 2.303RT/bF and R, F and T are the gas constant, Faraday constant and absolute temperature, respectively. The Tafel slope (b) is calculated from the polarization curves obtained at different temperatures. η is the overpotential.

$\Delta S^{\circ\#} = 2.3R\,[\log j + \Delta H_{el}^{\circ\#}/2.3RT - \log (nF\omega C_{OH^-})]$ ……(2)

Where, ω (= $k_B T/h$) is the frequency term and n = 2, k_B and h are the Boltamann constant and Plank's constant, respectively.

The estimated values of transfer coefficient (α), standard apparent enthalpy of activation $\Delta H_{el}^{\circ\#}$, standard enthalpy of activation ($\Delta H^{\circ\#}$) and entropy of activation ($\Delta S^{\circ\#}$) are given in Table 3. The thermodynamic parameters shows that the value of $\Delta H_{el}^{\circ\#}$ is minimum (35.1 kJmol^{-1}) for $La_{0.6}Cu_{0.4}CoO_3$ oxide film electrode. Also, it is observed that the value of activation energy decreases with the increase of applied potential and it is well satisfied by the equation (1). The highly negative values (-195.7 Jdeg^{-1} mol^{-1}) of $\Delta S^{\circ\#}$ indicate the role of adsorption in OER.

Table 4. Thermodynamic parameters for O_2 evolution on Ni/ $La_{1-x}Cu_xCoO_3$ ($0 \leq X \leq 0.8$) in 1 M KOH.

Electrode	**$\Delta H_{el}^{\circ\#}$ (kJ mol^{-1}) at E = 650 mV**	**$-\Delta S^{\circ\neq}$ (Jdeg^{-1} mol^{-1})**	**α**	**$\Delta H^{\circ\neq}$ (kJ mol^{-1})**
$LaCoO_3$	43.0	-184.9	0.7	68.3
$La_{0.8}Cu_{0.2}CoO_3$	45.3	-174.1	0.7	70.0
$La_{0.6}Cu_{0.4}CoO_3$	35.1	-195.7	0.5	52.3
$La_{0.4}Cu_{0.6}CoO_3$	42.3	-181.2	0.6	64.7
$La_{0.2}Cu_{0.8}CoO_3$	40.2	-182.7	0.5	58.3

4. CONCLUSION

In summary, simple and low cost perovskite-type materials have been developed for electrocatalysis of oxygen evolution reaction in alkaline medium. The X-ray diffraction study indicated the formation of almost pure perovskite phase of the material with hexagonal crystal geometry. The electrochemical investigations revealed that the substitution of Cu for La in the base oxide increased the electrocatalytic activity towards OER. The value being highest with 0.4 mol Cu-substitution (j_a= 111.2 mAcm^{-2}). The lowest value of activation ($\Delta H_{el}^{\circ\#}$ = 35.1 kJ mol^{-1}) also favours towards the better electrocatalytic activity of the material. The oxide electrode did not follow any regular trend in the case of roughness factor. However, the value was found to be highest with $La_{0.8}Cu_{0.2}CoO_3$ (R_F = 1244).

ACKNOWLEDGEMENTS

Authors are thankful to Department of Science and Technology (DST), New Delhi for financial support as Fast Track Scheme for Young Scientist (No.: SR/FT/CS–044/2009).

References

1. S. Chu and A. Majumdar, *Nature*, 488 (2012) 294-303.
2. Y. Zhu, W. Zhou, J. Yu, Y. Chen, M. Liu and Z. Shao, *Chem. Mater*., 28 (2016) 1691-1697.
3. D. J. Chen, C. Chen, Z. M. Baiyee, Z. P. SHao and F. Ciucci, *Chem. Rev*., 115 (2015) 9869-9921.
4. M. Armand and J. M. Tarascon, *Nature*, 451 (2008) 652-657.
5. W. G. Walter, E. L. Warren, J. R. McKone, S. W. Noettcher, Q. Mi, E. A. Santori and N. S. Lewis, Chem. Rev., 110 (2010) 6446-6473.
6. M. W. Kanan and D. G. Nocera, *Science*, 321 (2008) 1072-1075.
7. H. B. Gray, *Nat. Chem*., 1 (2009) 7-7.
8. Y. Cheng and S. P. Jiang, *Prog. Nat. Sci: Mat. Int*., 25 (2015) 545-553.
9. R. N. Singh, S. K. Tiwari, S. P. Singh, N. K. Singh, G. Poillerat and P. Chartier, *J. Chem. Soc. Faraday Trans*. 92 (1996) 2593-2598.
10. E. J. M. O'Sullivan and E. J. Calvo, In Electrode Kinetic Reaction, ed. R. G. Compton, Elsecier, Amsterdam, 1987.
11. S. Trasatti and G. Lodhi., In Electrodes of Conductive Metallic Oxides, Part B, ed. S. Trasatti, Elsevier, Amsterdam, 1981.
12. H. Wendt and G. Imarisio, *J. Appl. Electrochem*., 18 (1988) 1.
13. Y. Matsumoto, H Yoneyama and H. Tamura, *Chem. Lett*., (1975) 661; D. B. Meadowcroft, *Nature (London)*, 226 (1970) 848.
14. A. K. Ladovos and P. Pomonis, *J. Chem. Soc. Faraday Trans*., 87 (1991) 3291-3297.
15. J. O. M. Bockris and T. Otagawa, *J. Electrochem. Soc*. 131 (1984) 290-302.
16. J. Balej, *Int. J. Hydrogen Energy*, 10 (1985) 89-99
17. A. G.C. Kobussen, F. R. van Buren, T. G. M van Den Belt and H. J. A van Wees, *J. Electroanal Chem.*, 96 (1979) 123-125.
18. Y. Matsumoto, H. Manabe and E. Sato, *J. Electrochem Soc.* 123 (1980) 811-814.
19. H. Wendt and V. Plzak, *Electrochim .Acta* 28 (183) 27-34.
20. G. Fiori and C. M. Mari, *Int. J. Hydrogen Energy*, 7 (1982) 489-493.
21. Y. Terayoka, H. Kakebayashi, I. Moriguchi and S. Kagawa, *Chem. Lett*., (1991) 637-676.
22. K. Vidyasagar, J. Gopalkrishanan and C. N. R. Rao, *J. Solid State Chem*., 58 (1985) 29-37.
23. H. Taguchi, D. Matsuda and M. Nagao, *J. Am.. Ceram. Soc*., 76 (1992) 201
24. S. P. Sharibaa, P. J. Pomonis and A. J. Sdoukos, *J. Mater. Chem*., 1 (1991) 781-
25. J. K. Vassiliou, M. Hornbostel, R. Ziebarth and F. J. Disalvo, *J. Solid State Chemistry*, 81 (1989) 208-216.
26. S. K. Tiwari, P. Chartier and R. N. Singh, *J. Electrochem. Soc*., 142 (1995) 148-153.
27. A. N. Jain, S. K. Tiwari, R. N. Singh and P. Chartier, *J. Chem. Soc. Faraday Trans*., 91 (1995) 1871-1875.
28. R. N. Singh, A. N. Jain, S. K. Tiwari, G. Poillerat and P. Chartier, *J. Appl. Electrochem*., 25 (1995) 1133-1138.
29. R. N. Singh, S. K. Tiwari, S. P. Singh, A. N. Jain and N. K. Singh, *Int. J. Hydrogen Energy*, 22 (1997) 557-562.
30. S. K. Tiwari, J. F Koenig, G. Poillerat, P. Chartier and R. N. Singh, *J. Appl. Electrochem*., 28 (1998) 114-119.
31. A. N. Jain, S. K. Tiwari and R. N. Singh, *Ind. J. Chem*., 37A (1998) 125-129.
32. N. K. Singh, S.K. Tiwari, and R. N. Singh, *Int. J. hydrogen Energy*, 23 (1998) 775-780.
33. T. Sharma, N. K. Singh, S.K. Tiwari, and R. N. Singh, *Ind. J. Eng. Mat. Sci*. 5 (1998) 38-42.
34. N. K. Singh, B. Lal and R. N. Singh, *Int. J. hydrogen Energy*, 27 (2002) 885-893.
35. R. N. Singh, S. K. Tiwari, T. Sharma, P. Chartier and J. F. Koenig, *J. New Mat. Electrochem. Syst*., 2(1999) 65-69.

36. B. Lal, M. K. Raghunanda, M. Gupta and R. N. Singh, *Int. J. Hydrogen Energy* 30 (2005) 723-729.
37. C. Jin, X. Cao, L. Zhang, C. Zhang and R. Yong, *J. Power Sources*, 241 (2013) 225-230.
38. P. H. Benhangi, A. Alfantagi and E. Gyenge, *Electrochim. Acta*, 123 (2014) 42-50.
39. X. Cheng, E. Fabbri, M. Nachtegaal, I. E. Castelli, M. El Kazzi, R. Haumont, N. Marzari and T. J. Schmidt, *Chem. Mater*., 27 (2015) 7662-7672.
40. S. Egelund, M. Caspersen, A. Nikiferov and P. Moller, *Int. J. Hydrogen Energy*, 41 (2016) 10152-10160.
41. M. K. Yadav, Ritu Yadav, Priys Sharma and N. K. Singh, *Int. J. Electrochem. Sci*., 11 (2016) 8633-8645.
42. R. N. Singh, J. P. Pandey, N. K. Singh, B. Lal, P. Chartier and J. F. Koenig, *Electrochim. Acta*, 45 (2000)1911-1919.
43. N. Fradette and B. Marsan, *J. Electrochem. Soc*., 145 (1998) 2320-2327.
44. PH. Vermeiren, , R. Leysen, H. W. King, G. J. Murphy, and H. Vandenborre, *Int. J. Hydrogen Energy*, 12 (1987) 469-472.
45. R. N. Singh, J. P. Pandey and K. L. Anitha, *Int. J. Hydrogen Energy*, 18 (1993) 467-473.
46. S. Trasatti, in Electrochemical Hydrogen Technology, ed. H. Wendt, Elsevier, Amsterdam, 1990, p. 104.
47. S. P. Singh, R. N. Singh, P. Chartier and G. Poillerat, *Int. J. Hydrogen Energy*, 20 (1995), 203-210.
48. E. Gileadi, *Electrode Kinetics*, (VCH Publishers Inc., New York), 1993 p.151